

Comparison of spectral characteristics between EO-1 ALI and IRS-P6 LISS-III imagery

Xuehong Zhang^{1,2,*} and Qingjiu Tian²

¹School of Geography and Remote Sensing, Nanjing University of Information Science and Technology, Nanjing 210044, China

²International Institute for Earth System Science, Nanjing University, Nanjing 210093, China

Data from the Indian Remote Sensing Satellite (IRS) P6 have been widely used for integrated land and water resources management. To complement and substitute data measured from other similar satellites and obtain constant measurements of the Earth's surface features, we evaluated the spectral characteristics between IRS-P6 LISS-III, a sensor of IRS P6, and EO-1 ALI by comparing their top-of-atmosphere (TOA) reflectance and normalized difference vegetation index (NDVI) of three nearly simultaneous image pairs. In particular, due to the difference in NIR band design between LISS-III and ALI, the spectral characteristics of NIR band of LISS-III were compared with the two NIR bands of ALI. The results demonstrate that a distinct linear correlation exists between the spectral characteristics of LISS-III and ALI, with R^2 values ranging from 0.976 to 0.995 for TOA reflectance and from 0.992 to 0.997 for NDVI. Therefore, a mutual complementation and substitution of the TOA reflectance and NDVI between LISS-III and ALI images is feasible. Moreover, both TOA reflectance and NDVI of LISS-III are more similar to those of ALI at band 4 than to those of ALI at band 4P due to the difference in the two NIR bands of ALI.

Keywords: Normalized difference vegetation index, remote sensing satellite, spectral characteristics, top-of-atmosphere reflectance.

NUMEROUS satellite sensors are available for observing the Earth. There is an increasing need to use data from multiple sensors in order to obtain continuous measurements of the Earth's surface features. However, the quality of remotely sensed images is variable due to the atmospheric interference, different Sun-viewing geometry parameters, orbital parameters and imaging parameters, etc. Therefore, it is important to understand the difference between different types of sensors.

The Earth Observing One (EO-1) programme is a distinctive high-resolution sampling mission¹. EO-1 was launched on 21 November 2000; it carries three sensors – Atmospheric Corrector (AC), Hyperion and Advanced Land Imager (ALI). EO-1 has continually acquired quality

data from the beginning and it will continue to acquire images until 2016 (ref. 1). Therefore, data obtained by EO-1 can be used to validate other satellites data owing to the long operational period, e.g. using ALI data to validate or compare with Landsat 7 ETM+ (refs 2–6), MODIS^{3,4} and Landsat 5 TM^{7,8}.

The Indian Remote Sensing Satellite (IRS) P6 also called ResourceSat-1 was launched on 17 October 2003; it carries three optical cameras, i.e. Linear Imaging Self Scanner Sensor (LISS) III, Advanced Wide-Field Sensor (AWiFS) and a high-resolution multispectral sensor (LISS-IV). IRS-P6 is a mission primarily dedicated to agricultural applications in India⁹, whose payload was designed to provide continued remote sensing data services on an operational basis for integrated land and water resources management¹⁰. The data acquired by these sensors are widely used in many fields. For instance, LISS-III data are widely applied to inventory and assessment of wetlands^{11,12}, assessment of spatio-temporal dynamics of forest cover¹³, estimation of physical characteristics of lake system and seawater^{14–18}, retrieving leaf area index¹⁹, monitoring temporal variability in surface waterlogging²⁰ and so on.

In view of wide application of IRS-P6 data, to complement and substitute data measured from other similar satellites and further obtain constant measurements of the Earth's surface features, it is necessary to compare spectral characteristics between IRS-P6 and other satellites. Some studies have compared the spectral characteristics between IRS-P6 and other satellites such as Landsat 5 (ref. 21), Landsat 7 (ref. 21) and IRS-1D (ref. 22). Based on the analyses of orbital parameters, imaging features, spectral response characteristics, TOA reflectance and NDVI, the present communication compares the spectral characteristics between IRS-P6 LISS-III and ALI, to establish quantitative relationships between spectral characteristics of the two sensors. Moreover, it also aims to understand the spectral difference between the two sensors at near infrared (NIR) band due to the two narrow NIR bands of ALI.

There is little difference between EO-1 and IRS-P6 regarding the orbital parameters (Table 1). The imaging parameters of EO-1/ALI and IRS-P6/LISS-III are compared in Tables 1 and 2. The swath width of ALI and LISS-III are 37 and 141 km respectively, while spatial resolution of multiband of ALI and LISS-III are 30 and 23.5 m respectively. There are four similar bands between the two sensors, viz. bands 2–5.

Figure 1 shows the relative spectral response profiles between corresponding EO-1 ALI and IRS-P6 LISS-III spectral bands. Table 2 summarizes the spectral coverage of the two sensors. The IRS-P6 LISS-III bands are similar to the corresponding EO-1 ALI bands, except for band 4. The spectral range of LISS-III band 4 fully contains ALI band 4 and LISS-III band 4 overlaps ALI band 4P from 0.845 to 0.86 μm .

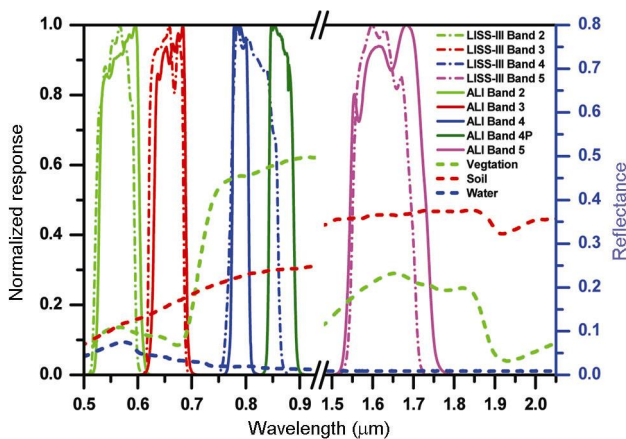
*For correspondence. (e-mail: zxhnbnu@gmail.com)

Table 1. ALI and LISS-III key specifications

| Platform | EO-1 | IRS-P6 |
|-------------------------------|------------------|---|
| Sensor | ALI | LISS-III |
| Launch date | 21 November 2000 | 17 October 2003 |
| Orbit type | Sun-synchronous | Sun-synchronous |
| Equatorial crossing time (AM) | 10:01 | 10:30 |
| Altitude (km) | 705 | 817 |
| Repeat cycle (days) | 16 | 24 |
| Inclination (°) | 98.2 | 98.7 |
| Cycles/day | 14.5 | 14.2 |
| Number of bands | 10 | 4 |
| Spatial resolution (m) | 10, 30 | 23.5 |
| Swath (km) | 37 | 141 |
| Spectral coverage (μm) | 0.4–2.5 | 0.5–1.75 |
| Pixel quantization (bits) | 12 | 7 (bands 2–4) 10 (band 5) transmission 7 bits |

Table 2. Spectral coverage of ALI and LISS-III sensors (μm)

| Band | ALI | LISS-III |
|------|-------------|-----------|
| 1P | 0.433–0.453 | |
| 1 | 0.450–0.515 | |
| 2 | 0.525–0.605 | 0.52–0.59 |
| 3 | 0.630–0.690 | 0.62–0.68 |
| 4 | 0.775–0.805 | 0.77–0.86 |
| 4P | 0.845–0.890 | |
| 5P | 1.200–1.300 | |
| 5 | 1.550–1.750 | 1.55–1.70 |
| 7 | 2.080–2.350 | |
| Pan | 0.480–0.690 | – |

**Figure 1.** Relative spectral response profiles of EO-1 ALI and IRS-P6 LISS-III in corresponding bands and typical signatures of few targets from the green to the SWIR region.

To effectively make a comparison of spectral characteristics, the near-simultaneous images available over sites having minimal cloud cover, high spatial uniformity, high solar elevation and many land-cover types should be selected. Following these criteria, three common image pairs (Figure 2 and Table 3) were selected from China for

this study. Each image pair has similar solar elevation. The difference in imaging time is about 30 min and it can be assumed that the imaging atmosphere condition does not obviously change for each image pair. The three image pairs were dated 29 September 2006, 23 April 2007 and 11 August 2007 respectively. These test sites contain land-cover types as follows: water, vegetation, bare soil, man-made and salt field.

To reduce the topographic effect on the comparison of spectral characteristics, very small sample regions for each land-cover type from the image pairs were selected. Each region selected has high spatial uniformity and the same land-cover type. Therefore, the statistical values, e.g. mean, of spectral features for each sample region in each image pair can be compared. This can effectively reduce the effect of error in the procedure of geometric correction. Finally, 28 sample regions were selected from the 3 image pairs with no less than 100 pixels for each sample region, including 8 water regions, 4 cropland regions, 4 forest regions, 8 soil regions, 2 manmade regions and 2 salt field regions.

The image processing included top-of-atmosphere (TOA) reflectance calculation and geometric correction. At first, the digital numbers were converted to at-aperture radiance using calibration coefficients. The TOA reflectance was then calculated using the radiance by formula as follows:

$$\rho_{\text{TOA}} = \frac{\pi L_{\lambda} d^2}{\text{ESUN}_{\lambda} \cos \theta_s}, \quad (1)$$

where ρ_{TOA} is the TOA reflectance, L_{λ} the at-aperture radiance, ESUN_{λ} the mean solar exoatmospheric irradiance, θ_s is the solar zenith angle (if we write α_s for the solar elevation angle, then the solar zenith angle $\theta_s = 90^\circ - \alpha_s$, and single value of solar elevation angle is used for the scene of interest for both LISS-3 as well as ALI sources), and d is the Earth–Sun distance in astronomical units.

Table 3. Coincident ALI and LISS-III image pairs in the present study

| Location | Date | Scene centre scan time (GMT) | Sensor | Path/row | Solar elevation (°) |
|---------------------------------|------------|------------------------------|----------|----------|---------------------|
| Dandong City, Liaoning Province | 2006/09/29 | 02 : 06 | ALI | 118/31 | 42.7 |
| | | 02 : 40 | LISS-III | 137/40 | 44.6 |
| Yancheng City, Jiangsu Province | 2007/04/23 | 02 : 16 | ALI | 119/37 | 59.1 |
| | | 02 : 52 | LISS-III | 135/47 | 64.1 |
| Golmud City, Qinghai Province | 2007/08/11 | 04 : 11 | ALI | 137/33 | 58.8 |
| | | 04 : 40 | LISS-III | 109/44 | 63.3 |

Table 4. Mean solar exoatmospheric irradiance of ALI and LISS-III ($W(m^2Sr\ \mu m)^{-1}$)

| Band | ALI | LISS-III |
|------|-------|----------|
| 2 | 1807 | 1848.92 |
| 3 | 1536 | 1576.79 |
| 4 | 1145 | 1093.38 |
| 4P | 955.8 | |
| 5 | 235.1 | 237.50 |

*Source: Refs 22 and 23.

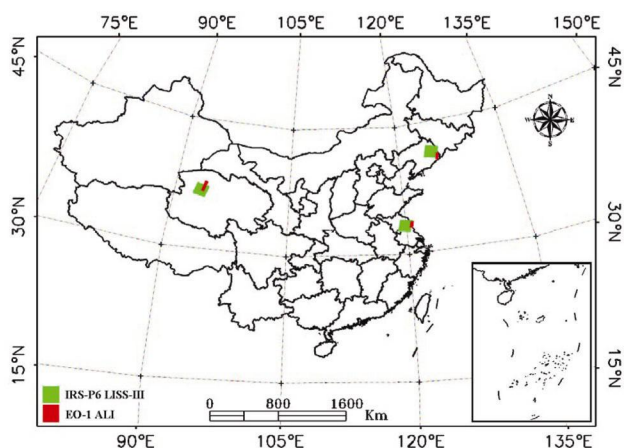


Figure 2. Overlaid area of ALI and LISS-III synchronization scenes within China.

The values of d are from Chander *et al.*²³. $ESUN_{\lambda}$ can be obtained from Table 4. TOA reflectance can remove the cosine effect of different solar zenith angles owing to the imaging time difference of data acquisitions. Meanwhile, TOA reflectance also offsets the differences in solar exoatmospheric irradiances induced by the spectral band coverage. The procedure of geometric correction usually carries out image resampling and this often reduces image quality. The nearest-neighbour interpolation was employed to perform geometric correction on IRS-P6 LISS-III images based on the EO-1 ALI data coordinates (Transverse Mercator Projection, WGS_1984_UTM_Zone) provided by International Scientific Data Service Platform (<http://www.gscloud.cn>).

The mean value of TOA reflectance at each band within each sample region was computed using ROI tools of ENVI version 4.7 digital image processing software (ITT Industries Inc., USA). The comparison of TOA reflectance was made at the corresponding bands over the 28 selected sample regions. Due to the two narrow NIR bands of ALI, i.e. band 4 and band 4P, TOA reflectance of LISS-III at band 4 was compared with the two NIR bands of ALI respectively. Figure 3 *a–e* demonstrates the results from these comparisons and Table 5 summarizes the relation between TOA reflectance of EO-1 ALI and IRS-P6 LISS-III. The ALI TOA reflectance is plotted on the x-axis and the LISS-III TOA reflectance is plotted on the y-axis. The 1 : 1 line is also plotted for reference, and a least squares fit has been made to the data in each band. Each data point on the scatter plots represents an ensemble average of all pixels in a given sample region and is colour-coded by land-cover types.

Figure 3 shows a distinct linear correlation between TOA reflectance of LISS-III and that of ALI for the corresponding bands, and all the coefficients of determination are close to 1. However, all the slope values are less than 1. Considering the 1 : 1 line, the area above the line represents the TOA reflectance of LISS-III greater than that of ALI, whereas the area below the line represents the opposite. The above results are consistent with the earlier studies^{2,21} comparing ETM+ and ALI as well as ETM+ and IRS-P6 LISS-III respectively^{2,21}. For instance, Figure 3 *a* summarizes the TOA reflectance comparison result for band 2. Although the R^2 value (0.9934) is close to 1, the slope (0.8773) is less than 1. According to the 28 sample regions of five land-cover types, TOA reflectance of LISS-III is obviously lower than that of ALI, except for water, especially for sample regions of bare soil and salt field. The comparison results of band 3 (Figure 3 *b*), and band 5 (Figure 3 *e*) are similar to that of band 2.

The comparison result for band 4 (see Figure 3 *c*), is similar to that of bands 2, 3 and 5, but the difference between the two sensors in band 4 is smaller than the above three bands. Figure 3 *d* compares TOA reflectance of LISS-III at band 4 with that of ALI at band 4P, in which R^2 value (0.9757) and slope (0.8684) are smaller than those of Figure 3 *c* ($R^2 = 0.9930$, slope = 0.9369), which compares TOA reflectance of LISS-III at band 4

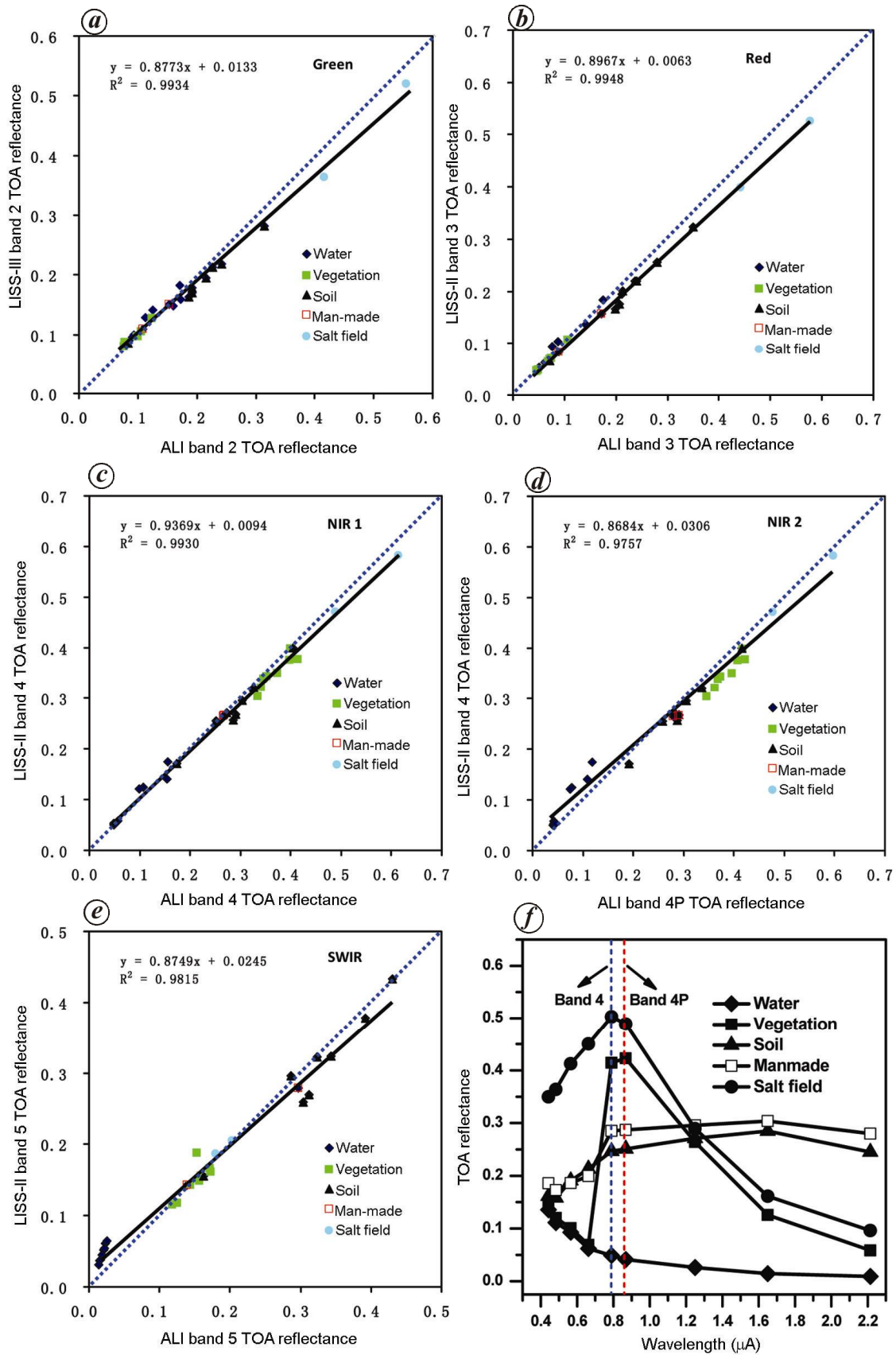


Figure 3. *a–e*, Scatter plots of mean TOA reflectance of LISS-III versus ALI at each sample region for each band; *f*, TOA reflectance curves of typical targets obtained from ALI sensor.

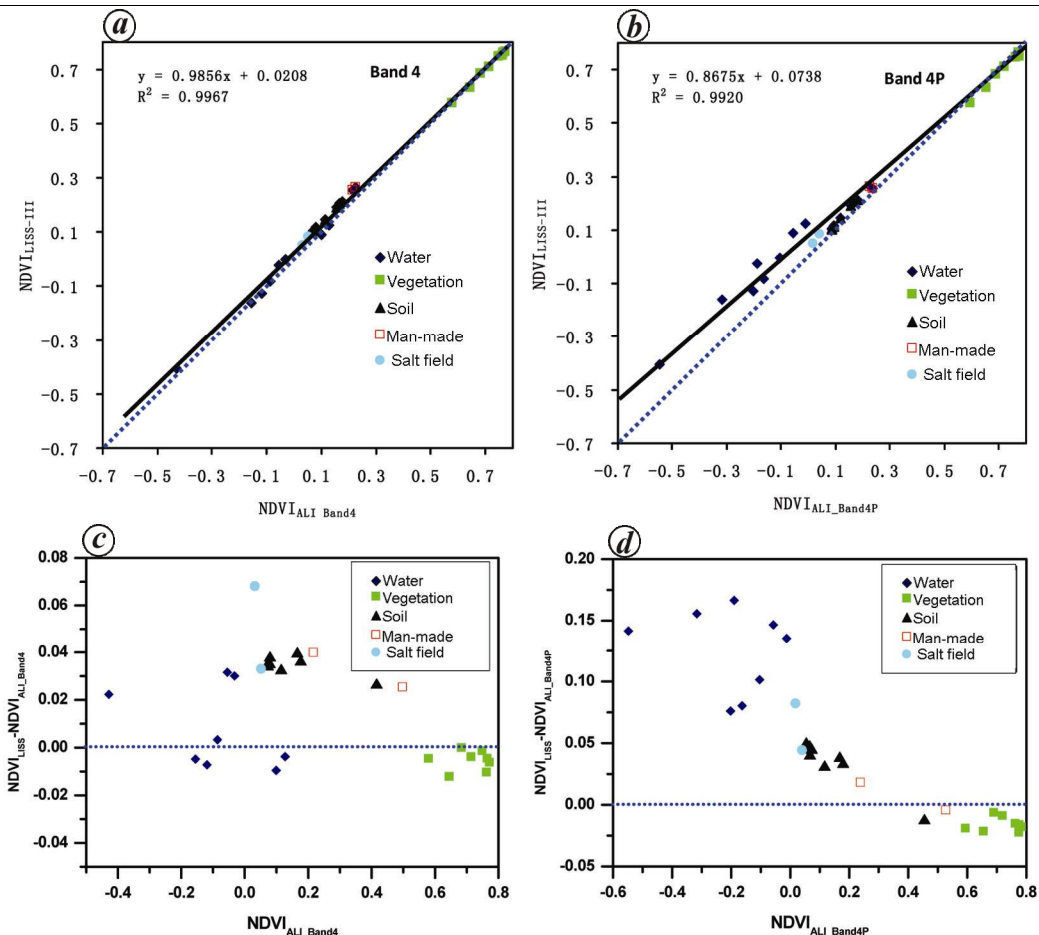


Figure 4. *a, b*, Scatter plots of mean NDVI of LISS-III versus ALI at each sample region; *c, d*, Absolute difference in NDVI between LISS and ALI as a function of NDVI of ALI.

Table 5. Relation between TOA reflectance and NDVI of EO-1 ALI and IRS-P6 LISS-III

| Spectral characteristics | Y/X | Expression | R ² |
|--------------------------|-------------------------------------|------------------------|----------------|
| TOA reflectance | IRS-P6-LISS-III-band2/ALI-band2 | $y = 0.8773x + 0.0133$ | 0.993 |
| | IRS-P6-LISS-III-band3/ALI-band3 | $y = 0.8967x + 0.0063$ | 0.995 |
| | IRS-P6-LISS-III-band4/ALI-band4 | $y = 0.9369x + 0.0094$ | 0.993 |
| | IRS-P6-LISS-III-band4/ALI-band4P | $y = 0.8684x + 0.0306$ | 0.976 |
| | IRS-P6-LISS-III-band5/ALI-band5 | $y = 0.8749x + 0.0245$ | 0.982 |
| NDVI | $NDVI_{LISS-III}/NDVI_{ALI-band4}$ | $y = 0.9856x + 0.0208$ | 0.997 |
| | $NDVI_{LISS-III}/NDVI_{ALI-band4P}$ | $y = 0.8675x + 0.0738$ | 0.992 |

with that of ALI at band 4. The x axis values are different between Figure 3 *c* and *d*, but the y-axis values (TOA reflectance of LISS-III at band 4) do not change. Therefore, the distance changes of points to the 1 : 1 line between Figure 3 *c* and *d* represent the differences in TOA reflectance of ALI between band 4 and band 4P. The distance of these land-cover types to the 1 : 1 line in Figure 3 *d* is longer than that in Figure 3 *c*, except for the salt field (because the points of the salt field in Figure 3 *c* are below the 1 : 1 line, the shortening of their distance to the line at band 4P (Figure 3 *d*) illustrates that their TOA re-

fectance decreases compared with band 4; Figure 3 *c*). The reason is that the TOA reflectance of vegetation, soil and man-made objects of ALI in band 4P is higher than that of ALI in band 4, and water and salt field have the opposite spectral characteristics (Figure 3 *f*). Moreover, this is consistent with the differences in relative spectral response profiles of ALI and reflectance curves of typical targets between band 4 and band 4P (Figure 1).

The vegetation index (VI) is related to the vegetation biomass, net primary productivity (NPP), coverage and leaf area index of canopies. Figure 4 and Table 5

summarize the comparison results of mean NDVI, obtained from LISS-III and ALI at each sample region, and show the absolute difference in NDVI between LISS and ALI as a function of NDVI of ALI for band 4 (Figure 4 *c*) and band 4P (Figure 4 *d*). The mean NDVI of ALI is plotted on the *x*-axis, and mean NDVI of LISS-III is plotted on the *y*-axis. The 1:1 line is also plotted for reference, and a least squares fit has been made to the data.

The R^2 value (0.9967) and slope (0.9856) of the regression model between $NDVI_{LISS-III}$ ($NDVI$ of LISS-III) and $NDVI_{ALI_Band4}$ ($NDVI_{ALI_Band4}$ denotes ALI NDVI calculated by band 4; see Figure 4 *a*) are closer to 1 compared to the regression model between $NDVI_{LISS-III}$ and $NDVI_{ALI_Band4P}$ ($NDVI_{ALI_Band4P}$ denotes ALI NDVI calculated by band 4P; see Figure 4 *b*), which R^2 value and slope being 0.9920 and 0.8675 respectively. This shows that the difference between $NDVI_{LISS-III}$ and $NDVI_{ALI_Band4}$ is smaller than that between $NDVI_{LISS-III}$ and $NDVI_{ALI_Band4P}$. The absolute difference plots in NDVI between LISS and ALI further prove the above results. The absolute difference in NDVI between $NDVI_{LISS-III}$ and $NDVI_{ALI_Band4}$ is from -0.02 to 0.07 for the typical land-cover types (Figure 4 *c*), whereas absolute difference in NDVI between $NDVI_{LISS-III}$ and $NDVI_{ALI_Band4P}$ is from -0.025 to 0.17 (Figure 4 *d*). Moreover, it has been found that a trend of the absolute difference in NDVI between $NDVI_{LISS-III}$ and $NDVI_{ALI_Band4P}$ decreases with the increase in NDVI, e.g. absolute difference of water, soil and vegetation increases in order.

In conclusion, a comparison was made between IRS-P6 LISS-III and EO-1 ALI by means of orbital parameters, imaging features and spectral response characteristics. Three common image pairs were selected from China, and 28 sample regions, including five land-cover types were also chosen. A comparative analysis was then made on the spectral characteristics (including TOA reflectance and NDVI) between the two sensors, and the mutual quantitative relation was established between these image pairs. The research results show the following: (i) A distinct linear correlation exists between spectral characteristics (TOA reflectance and NDVI) of IRS-P6 LISS-III and EO-1 ALI. Therefore, a mutual complementation and substitution of the TOA reflectance and NDVI between LISS-III and ALI images is feasible. However, TOA reflectance of LISS-III is obviously lower than that of ALI at the corresponding bands, except for water, especially for bare soil and salt field. (ii) With regard to the NIR band, the regression models of TOA reflectance between LISS-III and ALI are obviously different due to the two narrow NIR bands of ALI. It is found that the R^2 value and slope of the regression model of ALI at band 4 are closer to 1 compared to the regression model of ALI at band 4P. Both TOA and NDVI of LISS-III are more similar to those of ALI at band 4 than band 4P due to the difference in the two NIR bands of ALI. However, NIR band designs of most past and current remote sensors,

e.g. Landsat 5 TM, Landsat 7 ETM+, SPOT and Terra ASTER, are similar to band 4 of LISS-III, but the NIR band design of Landsat 8 OLI, which will be of importance in continuing the multi-decadal Landsat data record²⁴, is similar to band 4P of ALI. Hence, the differences in sensor spectral response and band design of NIR on the estimation of reflectance and NDVI should be taken into account when comparable measurements of satellite sensors for long-term monitoring of the Earth's environment are required.

1. Middleton, E. M. *et al.*, The Earth Observing One (EO-1) Satellite mission: over a decade in space. *IEEE J. Sel. Topics Appl. Earth Obs. Remote Sensing*, 2013, **6**, 243–256.
2. Chander, G., Meyer, D. J. and Helder, D. L., Cross calibration of the Landsat-7 ETM+ and EO-1 ALI Sensor. *IEEE Trans. Geosci. Remote Sensing*, 2004, **42**, 2821–2831.
3. Chander, G., Angal, A., Choi, T. and Xiong, X., Radiometric cross-calibration of EO-1 ALI with L7 ETM+ and Terra MODIS sensors using near-simultaneous desert observations. *IEEE J. Sel. Topics Appl. Earth Obs. Remote Sensing*, 2013, **6**, 386–399.
4. Thome, K. J., Biggar, S. F. and Wisniewski, W., Cross comparison of EO-1 sensors and other earth resources sensors to Landsat-7 ETM+ using Railroad Valley Playa. *IEEE Trans. Geosci. Remote Sensing*, 2003, **41**, 1180–1188.
5. Lobell, D. B. and Asner, G. P., Comparison of Earth Observing-1 ALI and Landsat ETM+ for crop identification and yield prediction in Mexico. *IEEE Trans. Geosci. Remote Sensing*, 2003, **41**, 1277–1282.
6. Donegan, S. J. and Flynn, L. P., Comparison of the response of the Landsat 7 Enhanced Thematic Mapper Plus and the Earth Observing-1 Advanced Land Imager over active lava flows. *J. Volcanol. Geotherm. Res.*, 2004, **135**, 105–126.
7. Petropoulos, G. P., Kontoes, C. C. and Keramitsoglou, I., Land cover mapping with emphasis to burnt area delineation using co-orbital ALI and Landsat TM imagery. *Int. J. Appl. Earth Obs. Geoinf.*, 2012, **18**, 344–355.
8. Pu, R., Bell, S., Meyer, C., Baggett, L. and Zhao, Y., Mapping and assessing seagrass along the western coast of Florida using Landsat TM and EO-1 ALI/Hyperion imagery. *Estuarine, Coastal Shelf Sci.*, 2012, **115**, 234–245.
9. Naval Gund, R. R., Jayaraman, V. and Roy, P. S., Remote sensing applications: an overview. *Curr. Sci.*, 2007, **93**, 1747–1766.
10. *IRS-P6 Users Data Handbook*, National Remote Sensing Agency, Hyderabad, India, 2003; <http://www.nrса.gov.in/Publications/handbooks.html> (accessed on 28 August 2014).
11. National Wetland Atlas, SAC/EPISA/ABHG/NWIA/ATLAS/34/2011, Space Applications Centre (ISRO), Ahmedabad, 2011; http://moef.nic.in/downloads/public-information/NWIA_Assam_Atlas.pdf (accessed on 28 August 2014).
12. Panigrahy, S., Murthy, T. V. R., Patel, J. G. and Singh, T. S., Wetlands of India: inventory and assessment at 1:50,000 scale using geospatial techniques. *Curr. Sci.*, 2012, **102**, 852–856.
13. Pattanaik, C., Reddy, C. S. and Reddy, P. M., Assessment of spatial and temporal dynamics of tropical forest cover: a case study in Malkangiri district of Orissa, India. *J. Geogr. Sci.*, 2011, **21**, 176–192.
14. Sheela, A. M., Letha, J., Joseph, S., Ramachandran, K. K. and Chacko, M., Computation of physical characteristics of a lake system using IRS P6 (LISS-III) imagery. *Int. J. Appl. Earth Obs. Geoinf.*, 2012, **14**, 221–232.
15. Prabakaran, S., Manonmani, R., Ramalingam, M., Vidhya, R. and Subramani, T., Decision of threshold values for extraction of turbidity for inland wetland using IRS P6 LISS III data. *Arab. J. Geosci.*, 2013, **6**, 109–114.

16. Sheela, A. M., Letha, J., Sabu, J., Ramachandran, K. K. and Justus, J., Detection of extent of sea level rise in a coastal lake system using IRS satellite imagery. *Water Resour. Manage.*, 2013, **27**, 2657–2670.
17. Chen, J., Hu, X. and Quan, W., Scale effects on chlorophyll-*a* concentration retrieved – assessment and validation using Indian Remote Sensing Satellite. *J. Indian Soc. Remote Sensing*, 2013, **41**, 105–116.
18. Sheela, A. M., Letha, J., Joseph, S., Ramachandran, K. K. and Sanalkumar, S. P., Trophic state index of a lake system using IRS (P6-LISS III) satellite imagery. *Environ. Monit. Assess.*, 2011, **177**, 575–592.
19. Pandya, M. R., Chaudhari, K. N., Singh, R. P., Sehgal, V. K., Bairagi, G. D., Sharma, R. and Dadhwal, V. K., Leaf area index retrieval using IRS LISS-III sensor data and validation of MODIS LAI product over Madhya Pradesh. *Curr. Sci.*, 2003, **85**, 1777–1782.
20. Singh, S. K. and Pandey, A. C., Geomorphology and the controls of geohydrology on waterlogging in Gangetic Plains, North Bihar, India. *Environ. Earth Sci.*, 2014, **71**, 1561–1579.
21. Chander, G., Michael, J. C. and Pasquale, L. S., Evaluation and comparison of the IRS-P6 and the Landsat sensors. *IEEE Trans. Geosci. Remote Sensing*, 2008, **46**, 209–221.
22. Pandya, M. R., Singh, R. P., Chaudhari, K. N., Murali, K. R., Kirankumar, A. S., Dadhwal, V. K. and Parihar, J. S., Spectral characteristics of sensors onboard IRS-1D and P6 satellites – estimation and their influence on surface reflectance and NDVI. *J. Indian Soc. Remote Sensing*, 2007, **35**, 333–350.
23. Chander, G., Markham, B. L. and Helder, D. L., Summary of current radiometric calibration coefficients for Landsat MSS, TM, ETM+, and EO-1 ALI sensors. *Remote Sensing Environ.*, 2009, **113**, 893–903.
24. Irons, J. R., Dwyer, J. L. and Barsi, J. A., The next Landsat satellite: the Landsat data continuity mission. *Remote Sensing Environ.*, 2012, **122**, 11–21.

ACKNOWLEDGEMENTS. This study was supported by the National Natural Science Foundation of China (Grant no. 41201461), the Jiangsu Government Scholarship and the National Science and Technology Major Project, China (Grant no. 30-Y20A01-9003-12/13).

Received 10 August 2014; revised accepted 1 October 2014

Climate change impact on design and costing of soil and water conservation structures in watersheds

B. Krishna Rao^{1,*}, R. S. Kurothe¹, P. K. Mishra², Gopal Kumar¹ and V. C. Pande¹

¹Central Soil and Water Conservation Research and Training Institute, Research Centre, Vasad 388 306, India

²Central Soil and Water Conservation Research and Training Institute, 218 Kaulagarh Road, Dehradun 248 195, India

A study was carried out to determine the effect of climate change on design rainfall and its effect on design and costing of soil and water conservation structures

in watersheds. For this study, the micro watershed located at Central Soil and Water Conservation Research and Training Institute, Research Centre, Research farm, Vasad was selected and rainfall data from 1957 to 2012 was used. The analysis showed that as a result of climate change, there is significant increase in number of extremely heavy rainfall days as well as rainfall amount. The design rainfall of various soil and water conservation structures has increased by 11%, 30% and 38% for design of staggered contour trenches, contour bunds and check dams respectively. The cost of construction of staggered contour trenches, contour bunds and check dams in watersheds has increased by 26%, 28% and 12% respectively. This study reveals that, there is a need to account for design and costing of soil and water conservation structures in the light of the climate change and a relook into the watershed programmes of the central Gujarat region of India.

Keywords: Climate change, design and costing, soil and water conservation structures, watersheds.

THE rainfall received in an area is an important factor in determining the amount of water available to meet various demands, such as agricultural, industrial, domestic supply and hydroelectric power generation. The global climatic data analysis clearly confirms a change in the climate¹. In India, too, the effect of climate change on rainfall, rainy days and water resources has been studied, which bears testimony to changes in these parameters over a long-term basis^{2–5}. Global climate changes may also influence long-term rainfall patterns impacting the availability of water, along with the increasing occurrences of droughts and floods. Studies^{2,6–10} show that, in general, the frequency of more intense rainfall events in many parts of Asia has increased, whereas the number of rainy days and total annual precipitation have decreased. Due to climate change impact, the irrigated maize, wheat and mustard in the northeastern (NE) and coastal regions, and rice, sorghum and maize in the Western Ghats (WG), may lose¹¹. Impacts of climate change and climate variability on the water resources affect the stream hydrology. Stream flows may rise drastically in the monsoon season, but will decrease in the non-monsoon season due to the projected future climate change^{12,13}.

The watershed management programme (WMP) is aimed at managing the precipitation (rainfall) in such a manner that it reduces runoff controls flood and helps in water harvesting (surface or subsurface) so as to be used during lean period for successfully raising the crops, and for other uses such as aquaculture or livestock, or both. It also maintains soil fertility, and does not accelerate soil loss. The watershed management programme provides livelihood support to the farmers as well. The watershed-based rural development management programmes are

*For correspondence. (e-mail: b_krishnarao@rediffmail.com)